

# THz emission from Co/Pt bilayers with varied roughness, crystal structure, and interface intermixing

G. Li<sup>1\*†</sup>, R. Medapalli<sup>2\*</sup>, R.V. Mikhaylovskiy<sup>1</sup>, F.E. Spada<sup>2</sup>, Th. Rasing<sup>1</sup>, E. E. Fullerton<sup>2</sup>,  
and A.V. Kimel<sup>1,3</sup>

[1] *Radboud University, Institute for Molecules and Materials, Heyendaalseweg 135, Nijmegen, The Netherlands.*

[2] *Center for Memory and Recording Research, University of California, San Diego, La Jolla, California 92093-0401, USA.*

[3] *Moscow Technological University, MIREA, Vernadsky Ave. 78, Moscow 119454, Russia.*

**Femtosecond laser excitation of a Co/Pt bilayer results in the efficient emission of picosecond THz pulses. Two known mechanisms for generating THz emission are spin-polarized currents through a Co/Pt interface, resulting in helicity-independent electric currents in the Pt layer due to the inverse spin-Hall effect and helicity-dependent electric currents at the Co/Pt interface due to the inverse spin-orbit torque effect. Here we explore how roughness, crystal structure and intermixing at the Co/Pt interface affect the efficiency of the THz emission. In particular, we varied the roughness of the interface, in the range of 0.1-0.4 nm, by tuning the deposition pressure conditions during the fabrication of the Co/Pt bilayers. To control the intermixing at the Co/Pt interface a 1-2 nm thick  $\text{Co}_x\text{Pt}_{1-x}$  alloy spacer layer was introduced with various compositions of Co and Pt. Finally, the crystal structure of Co was varied from face centered cubic to hexagonal close packed. Our study shows that the roughness of the interface is of crucial importance for the efficiency of helicity-dependent THz emission induced by femtosecond laser pulses. However, it is puzzling that intermixing while strongly enhancing the helicity-independent THz emission had no effect on the helicity-dependent THz emission which is suppressed and similar to the smooth interfaces.**

## (1) Introduction

For the last two decades, optical manipulation and excitation of magnetization dynamics at the picosecond and sub-picosecond timescales has been an active research field in magnetism [1-3], triggered by the seminal observation of ultrafast demagnetization of a thin Ni-film by a sub-100-fs laser pulse [4]. This demagnetization occurred much faster than any elementary interactions involving spins known at the time. Together with an intense search for the mechanisms of the ultrafast demagnetization, these first experiments also launched debates about the role of artifacts in ultrafast time-resolved measurements and the validity of the conclusions of these initial experiments [5-6]. These discussions motivated the development of new probes for ultrafast magnetization dynamics and resulted, in particular, in an elegant proposal to employ THz time-domain emission spectroscopy, which relies on the fact that any magnetic dipole change must be accompanied by an emission of electromagnetic radiation [7-9]. However, the application of THz time-domain emission spectroscopy for the study of ultrafast magnetization dynamics in magnetic multilayers led to rather unexpected results – the THz electric field emitted as the result of the laser induced demagnetization of Fe/Pt bilayers

\* Both authors performed equal amounts of work into the paper

† Contact: Qiao.Li@science.ru.nl

was stronger than the THz electric field emitted as the result of the demagnetization of a single Fe-film [10]. It was shown that ultrafast demagnetization generates a spin-polarized current from Fe to Pt, where, as a result of strong spin-orbit interaction, the spin-polarized current pulse was transformed to a charge current pulse is a more efficient source of THz emission than the magnetization dynamics itself. This mechanism for spin-to-charge conversion is known as the inverse spin-Hall effect. The THz emission did not depend on the polarization of light and the phase of the emitted THz radiation could be changed by 180-degrees by a magnetization reversal. These findings resulted in the development of new THz emitters based on heat-driven spin-polarized currents [11-14].

The first experiments on ultrafast laser-induced demagnetization, the latter not depending on the polarization of light, also inspired the search for ultrafast polarization dependent effects of light on magnetism. Although many groups tried, demonstration of an ultrafast polarization-dependent effect of light on magnets remained elusive, raising doubts about the feasibility of this phenomenon [15-17]. The first effect of circularly polarized femtosecond laser pulses on spins in a magnetic medium was discovered in the dielectric canted antiferromagnetic  $\text{DyFeO}_3$  and later demonstrated in a broad class of materials, including dielectric compensated antiferromagnets, dielectric and metallic ferrimagnets as well as ferromagnetic semiconductors [18-22]. Also in the case of polarization dependent effects of light on spins, THz time-domain emission spectroscopy was shown to be a powerful tool demonstrating the vectorial control of spins in antiferromagnetic  $\text{NiO}$  [23]. In Ref. [24], it was demonstrated that polarization dependent THz emission from ferromagnetic Co-films can be dramatically enhanced by growing a thin capping layer of Pt on top of the Co. The effect was explained to result from a helicity-dependent femtosecond laser-induced rotation of the magnetization of Co in the plane of the sample which, due to the inverse spin-orbit torque, generates a femtosecond pulse of electric current at the Co/Pt interface. This current generates a polarization dependent emission of THz radiation. This observation opens up appealing opportunities for fundamental studies of THz spintronics. In conventional spintronic devices, the direction of the current is controlled by both voltage and magnetic field. At the same time Huisman *et al.* [24] showed that the direction of sub-picosecond current pulses can be changed in a contactless manner, without applying a voltage, by simply changing the helicity of the excitation light.

Although it is clear that the polarization-dependent and polarization-independent THz emission from Co/Pt bilayers should depend on the properties of the interface between the Co and Pt layer, it still remains unclear if and how the roughness, crystal structure, and intermixing at this interface play any role in the process of the THz generation. In this paper we explore helicity-dependent (HD) [24] and helicity-independent (HI) [10] THz emission generated from Co/Pt with varying interface properties. We first fabricated amorphous Co/Pt bilayers by magnetron sputtering at various deposition pressures to vary the roughness at the Co/Pt interface. The quality of the interface was varied from a smooth to a relatively rough interface by varying the deposition chamber pressure from 3 mTorr to 40 mTorr. We then fabricated  $\text{Co}/\text{Co}_x\text{Pt}_{1-x}/\text{Pt}$  bilayers where the Co and Pt layers are separated by a 1 and 2 nm thick  $\text{Co}_x\text{Pt}_{1-x}$  alloy spacer layer with  $x$  being 25, 50, and 75. In these samples we studied the role of intermixing between Co and Pt atoms at the interface. Finally, we fabricated Co/Pt via epitaxial sputtering deposition where the Co was grown in the face centered cubic (FCC) or hexagonal close packing (HCP)

structure. In these samples we studied the role of the crystal structure and magnetic anisotropy on the observed laser-induced HI and HD THz emission. We found that the interfacial roughness affects the HI THz emission, but more importantly, plays a crucial role for the generation of the HD THz emission. We also found that the  $\text{Co}_x\text{Pt}_{1-x}$  alloy spacer layer, *i.e.* intermixing, has an amplification effect on the HI THz emission, but no effect on the HD THz emission. In addition, we did find a strong dependence of the HI THz emission in HCP Co/Pt with respect to the easy axis. For both the FCC and HCP Co/Pt we found no difference in the THz emission compared to the textured Co/Pt bilayer grown at 3 mTorr.

## (2) Sample Fabrication and Characterization

### (a) Interfacial Roughness Series

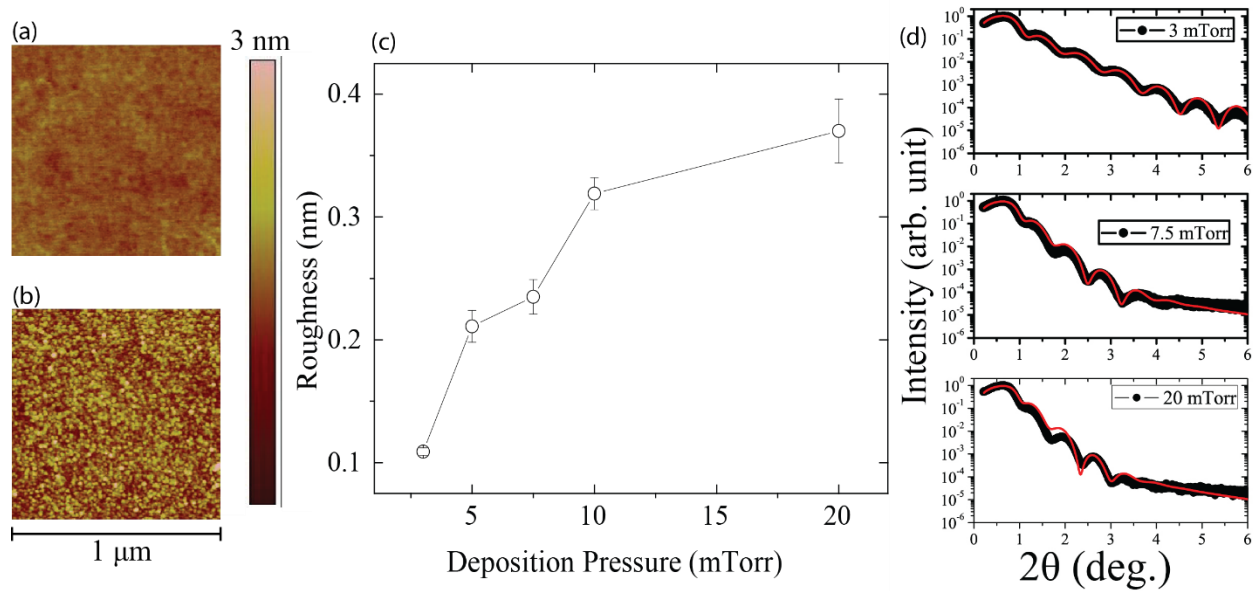


Figure 1 AFM images of the surface of sputter-deposited Co films grown on glass substrates at an Ar deposition pressure of (a) 3 mTorr and (b) 20 mTorr. (c) AFM root-mean-square roughness of the surface of the Co films grown at various deposition pressures. (d) The X-ray reflectometry signal of Co/Pt bilayers where the Co layer was grown at deposition pressures 3, 7.5, and 20 mTorr with the intensity plotted in logarithmic scales.

Using magnetron sputtering we fabricated polycrystalline Co/Pt bilayers on soda lime glass with varying interface roughness. For our study we fixed the thickness of both Co and Pt to 10 and 3 nm, respectively. Simultaneously, we fabricated Co-films (without Pt layer) for reference studies. To achieve a precise control over the roughness at the Co/Pt interface, for the growth of the Co layer we varied the Ar sputtering pressure from 3-40 mTorr. As the sputtering pressure increases, scattering of the sputtered Co atoms with the Ar atoms in the gas leads to a reduction of the average kinetic energy of the deposited atoms and the motion of Co atoms becomes more random. This results in a low surface mobility of the deposited atoms at high pressures and increased effects of self-shadowing. As the deposition evolves dome shaped grains are formed with well-defined grain boundaries known as zone-1 growth in thin-film deposition [25,26]. For the Pt layer, we kept the Ar-sputter pressure at 3 mTorr to form a dense capping layer. We find that the Co interfacial roughness increases with Ar pressure as expected.

Figures 1(a,b) show the atomic force microscopy (AFM) images of the reference Co samples without the Pt capping layer, revealing the change in growth morphology from a smooth surface to a grain like structure. Figure 1(c) shows the evolution of the AFM root-mean-square roughness of the Co surface with Ar sputtering pressure, showing a monotonic increase the roughness with Ar sputter pressure.

The X-ray reflectometry measurements on the Co/Pt bilayers shown in Fig. 1(d) are consistent with the AFM results. The strong suppression in the oscillations at higher angles for samples grown at higher deposition pressures confirms that interfacial roughness indeed increases with increasing deposition pressure.

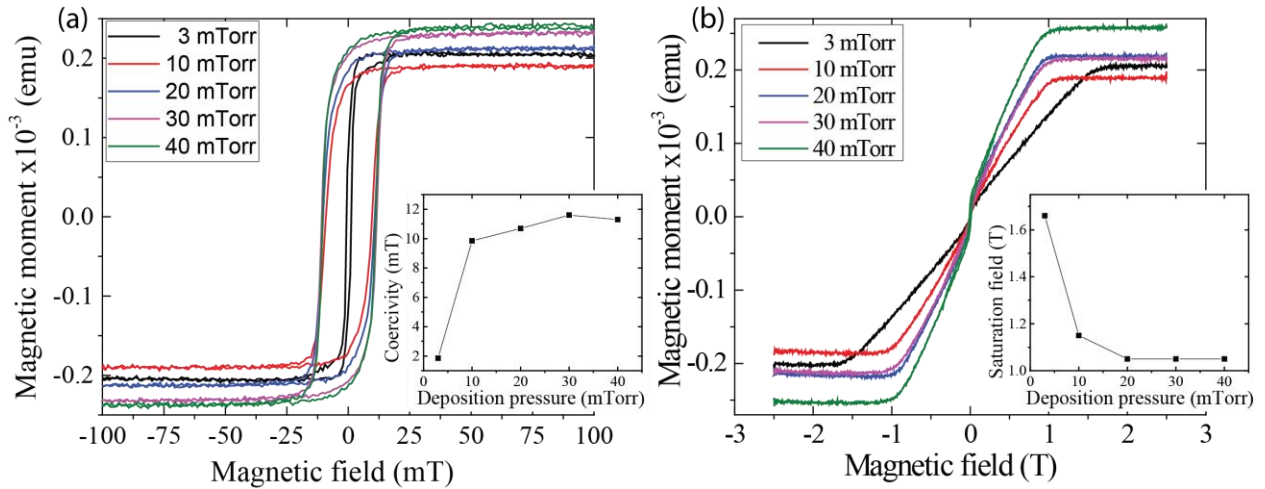


Figure 2 (a) Magnetic hysteresis loops measured in the in-plane magnetic field with the help of a vibrating sample magnetometer. (inset) The coercive field of each hysteresis loop measured in the in-plane magnetic field. (b) Similar magnetic hysteresis loop measurements but with the out-of-plane magnetic field. (inset) The strength of the applied out-of-plane magnetic field corresponding to the saturation magnetization.

For the magnetic characterization of the samples with varying roughness we used vibrating sample magnetometry and measured the magnetic hysteresis loop in an external magnetic field (see Fig. 2). The measurements were performed with the external magnetic field oriented either in-plane or out-of-plane of the sample. Figs. 2(a,b) summarize the in-plane and out-of-plane magnetometry measurements, respectively, obtained for Co/Pt bilayers grown at 3 mTorr up to 40 mTorr deposition pressures. The in-plane magnetization can be reversed and saturated by applying a rather small magnetic field of 12 mT, while the out-of-plane magnetization requires a much stronger applied magnetic field of more than 1.7 T. The inset of Fig. 2(a) summarizes how the in-plane coercive field depends on the deposition pressure. The inset of Fig. 2(b) shows how the deposition pressure affects the strength of the out-of-plane magnetic field corresponding to the saturation of the magnetization.

The magnetic properties change drastically between samples that were grown at a deposition pressure of 3 mTorr and 10 mTorr, as reflected in Fig. 2. Firstly, for Co/Pt grown at 3 mTorr and 10 mTorr the in-plane magnetic coercivity increases from 1.85 mT to 9.85 mT, respectively. The samples grown at deposition pressures larger than 10 mTorr show smaller changes in coercivity [27]. This is expected as the well-defined grain boundaries in high-pressure growth can

effectively pin the domain walls during reversal. Secondly, the out-of-plane magnetic saturation for Co/Pt grown at 3 mTorr and 10 mTorr drops from 1.66 T to 1.15 T, respectively. The decrease in the out-of-plane saturation field is somewhat unexpected as it should be dominated by the thin-film shape anisotropy. However, a granular microstructure can lower the overall effective shape anisotropy making the film easier to saturate with an external magnetic field.

## (b) Intermixed Interface

To explore the effects of chemical intermixing at the interface we sputter deposited the multilayer stack Co(10 nm)/Co<sub>x</sub>Pt<sub>1-x</sub>(1 or 2 nm)/Pt(3 nm) onto glass substrates. Note that for the study of the intermixing effect, on THz emission, all the layers including the spacer ones were deposited at a deposition pressure of 3 mTorr. The Co<sub>x</sub>Pt<sub>1-x</sub> layers were formed by co-deposition and the values of  $x = 0.25, 0.50$  and  $0.75$  were formed by adjusting the deposition conditions.

## (c) Epitaxial FCC-Co and HCP-Co

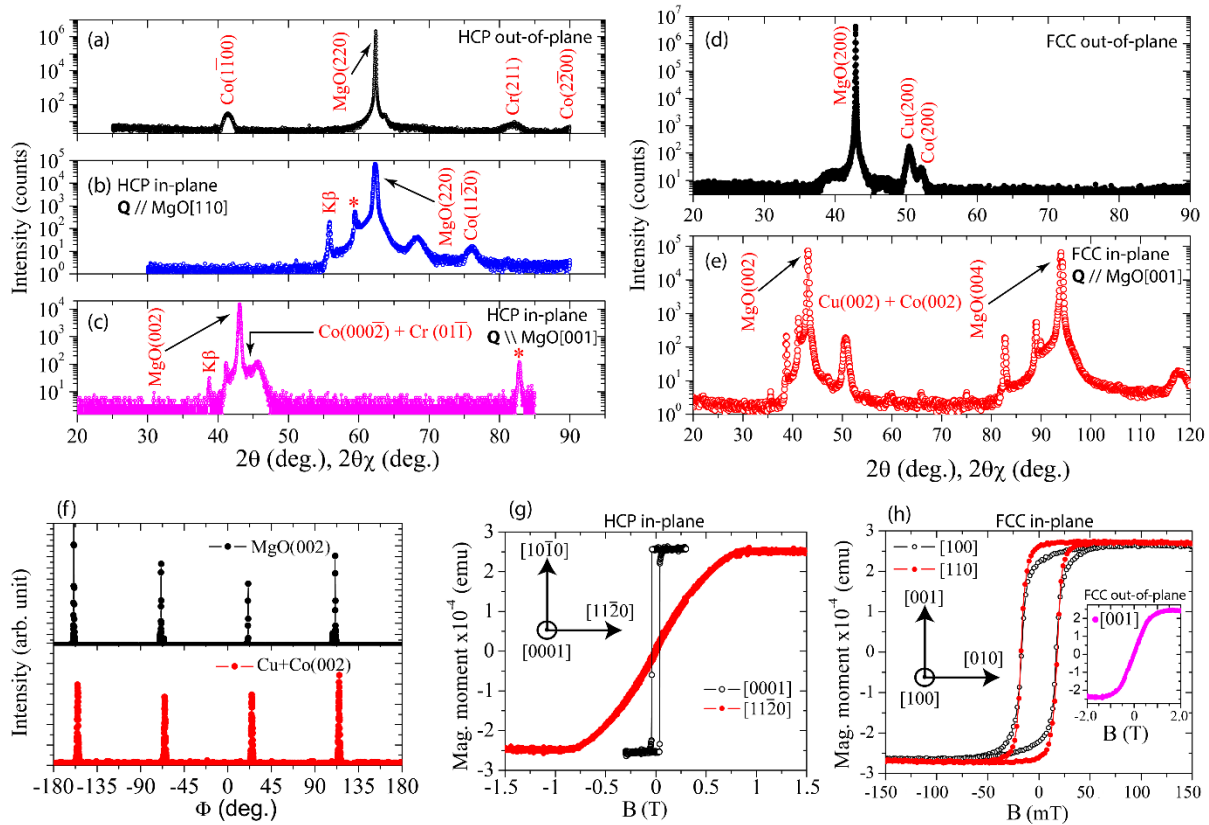


Figure 3 The intensities of (a-e) are given in logarithmic scales. (a) The out-of-plane X-ray diffraction spectrum of the HCP-Co film. (b) The in-plane spectrum where the scattering vector  $\mathbf{Q}$  (the vector pointing along the bisection of the incoming and scattered beam) is along the MgO[110] direction, and (c) where  $\mathbf{Q}$  is along the MgO[001] direction. The X-ray diffraction spectra of (d) the out-of-plane and (e) in-plane FCC-Co film with  $\mathbf{Q}$  along the MgO[001] direction. Note that the incident x-ray angle was fixed at  $0.6^\circ$  from the surface when the in-plane spectra

*was recorded. (f)  $\varphi$ -scans of the MgO(002) (top) and Cu(002)+Co(002) (bottom) families of peaks. (g) In-plane Magnetic hysteresis loops of (g) the HCP-Co and (h) FCC-Co films along various crystallographic directions.*

To explore the role of the crystal symmetry at the Co/Pt interface we grew epitaxial Co-films onto single-crystalline MgO substrates. Two particular lattice structures of Co were studied: HCP-Co(10-10) and FCC-Co(100) films. The HCP-Co films were grown on Cr(211)-buffered MgO(110) single-crystal substrates with the following structure MgO(110)/Cr(5 nm)/Co(10 nm)/Pt(3 nm) [28]. The Cr-seed layer was grown at 300 °C into the body-centered cubic (BCC) structure oriented along BCC(211). The subsequent Co layer was deposited at 200 °C and capped with a 3 nm Pt-layer at room temperature, resulting in the easy axis of the magnetic anisotropy oriented in-plane along HCP-Co(0001). The epitaxial growth is confirmed by x-ray diffraction, measurements are presented in Figs. 3(a-c) for both the out-of-plane and in-plane scattering geometries. The magnetic hysteresis loops for the in-plane and out-of-plane magnetic fields are shown in Fig. 3(g).

Using Cu(200)-buffered MgO(100) single-crystal substrates we obtained epitaxial FCC-Co with the following multilayer stacks MgO(100)/Cu(20 nm)/Co(10, or 15 nm)/Pt(3 nm). The Cu-seed layer was grown at 350 °C and oriented along FCC(200). The subsequent Co and Pt layers were grown at room temperature resulting in FCC-Co(200) oriented along the  $a$ -axis. The out-of-plane scattering of the 15 nm Co film is shown with the Cu(200) and FCC-Co(200) peaks. The X-ray diffraction signals of both the FCC and HCP crystal structures are in good correspondence with those of the previously measured FCC-Co and HCP-Co in Ref. [29]. The magnetic hysteresis loops for the out-of-plane and in-plane magnetic fields are shown in Fig. 3(h). Note that prior to the deposition of the films the substrates were heated at 600 °C for an hour under vacuum to obtain clean surfaces. Moreover, the base pressure throughout the deposition of all the samples was at  $3 \times 10^{-8}$  Torr.

### (3) Experimental method

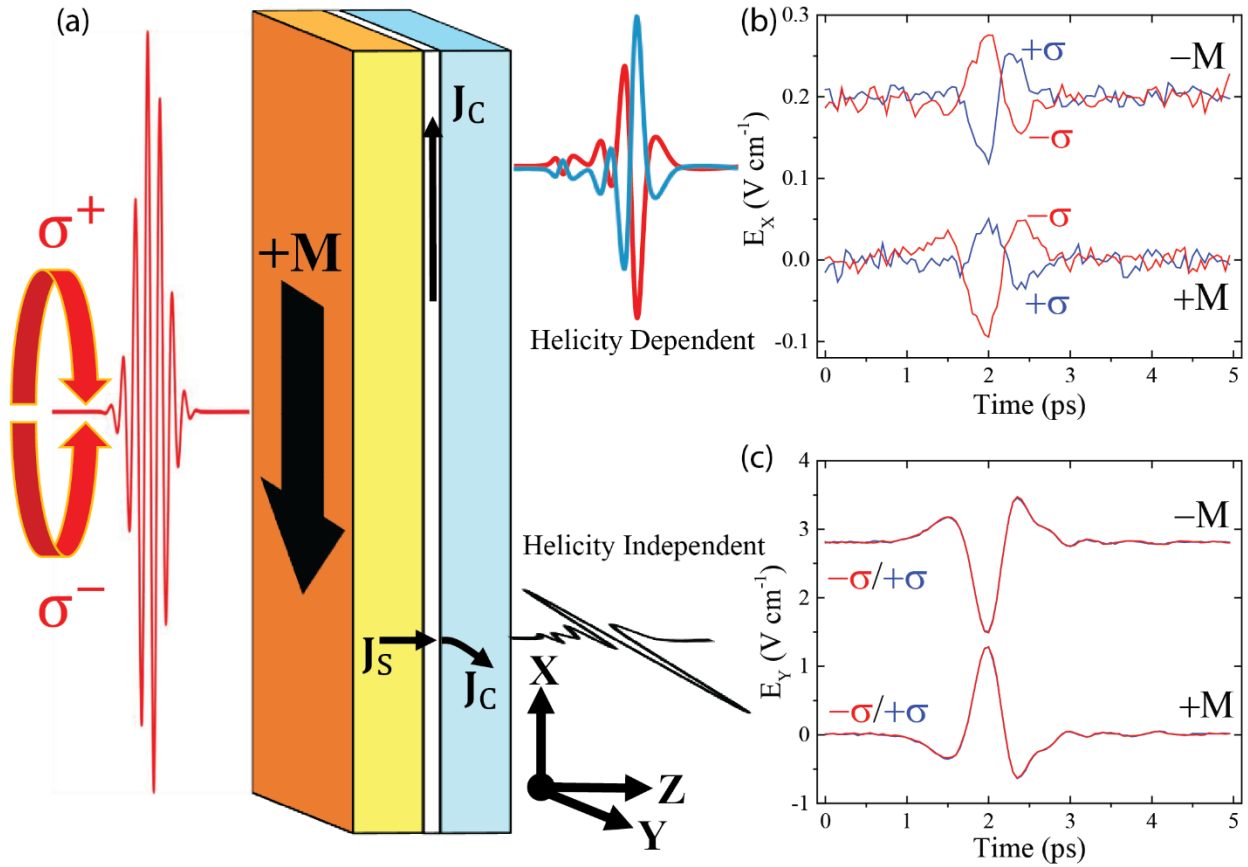


Figure 4 (a) A schematic illustration of the ultrafast photocurrent generation THz emission. The graphs on the right show the time traces of the electric field of (b) the helicity-dependent (HD) and (c) helicity-independent (HI) THz emission exited by circularly polarized ( $\pm\sigma$ ) light. In both cases, the THz electric field can be controlled by an external magnetic field. The figures also shows how reversal of the magnetization aligned along the  $\hat{x}$ -axis ( $\pm M$ ) affects the time traces of the emitted THz electric field. The curves measured for  $-M$  are shown with an off-set of 0.2V/cm for  $E_x$  in panel (b) and of 0.29 V/cm for  $E_y$  in panel (c).

A schematic depiction of the experimental geometry is shown in Fig. 4(a). To excite the photocurrents in the Co/Pt bilayer, we used a 40 fs circularly polarized laser pulse with a central wavelength of 800 nm and a pulse energy of 20  $\mu$ J, focused onto a 2 mm spot. An external magnetic field was applied in the plane of the sample to saturate its magnetization along the  $\pm\hat{x}$ -axis (see coordinate system in Fig. 4(a)). The emitted THz radiation from the sample was focused onto a 1-mm-thick ZnTe crystal using gold coated parabolic mirrors. The time-resolved electric field was then obtained via electro-optical sampling in the 1-mm-thick ZnTe crystal. The setup is similar to the one described in Ref. [30] and all experiments were all performed at room temperature.

We chose the coordinate system such that the propagation of the THz radiation was along the  $\hat{z}$ -axis and the external magnetic field was applied in-plane of the sample along the  $\hat{x}$ -axis. To measure the polarization of the THz radiation we employed two wire-grid polarizers. The axis of the first polarizer was fixed parallel to the  $\hat{y}$ -axis while the axis of the second polarizer was

rotated  $\pm 45$  degrees with respect to the axis of the first polarizer. This allowed us to determine the  $\hat{x}$  and  $\hat{y}$  components of the THz polarization. If the magnetization of the sample is aligned along the  $\hat{x}$ -axis, the THz emission from the HI and the HD photocurrents could be distinguished by detecting the THz signals (see Figs. 4(b,c)) with the electric field along the  $\hat{y}$ - and  $\hat{x}$ -axis, respectively.

The mechanism for generating the HI THz electric field is based on the generation of spin-polarized hot electrons in Co due to the heat driven ultrafast demagnetization [31]. This spin-polarized current flows from Co to Pt where it is converted into a charge current via the inverse spin-Hall effect [32,33]. The direction of the charge current  $\mathbf{J}_c$  is determined by the magnetization  $\mathbf{M}$ , the spin-polarized current flow  $\mathbf{J}_s$ , and the spin-Hall angle  $\alpha$ :  $\mathbf{J}_c \propto \alpha \mathbf{J}_s \times \mathbf{M}$ . The mechanism for the generation of the HD THz electric field is fundamentally different, since it requires circularly polarized light. The circularly polarized light will have a HD effect on the magnetization of Co, resulting a spin-orbit torque acting on the spins of Co at the interface with Pt [34,35]. The breaking of inversion symmetry is essential for the coupling of the optically induced spin dynamics and the generation of interfacial HD photocurrents [36,37]. The direction of the photocurrent in this mechanism is determined by the magnetization  $\mathbf{M}$ , the helicity of the light  $\sigma$ , and the direction along which the space inversion symmetry is broken (here given by the normal vector  $\mathbf{n}$ ):  $\mathbf{J}_c \propto \mathbf{n} \times (\mathbf{M} \times \sigma)$ .

In our analysis of the experimental data we retrieve the averaged HD THz ( $E^{HD}$ ) and HI THz ( $E^{HI}$ ) signals as

$$E^{HD} = \frac{1}{4}(E^{+\sigma+M} - E^{-\sigma+M} - E^{+\sigma-M} + E^{-\sigma-M}), \quad (1)$$

$$E^{HI} = \frac{1}{4}(E^{+\sigma+M} + E^{-\sigma+M} - E^{+\sigma-M} - E^{-\sigma-M}). \quad (2)$$

Here  $E^{HD}$  and  $E^{HI}$  are the polarized HD and HI THz electric field.



## (4) THz emission results

### (a) Interfacial Roughness Series

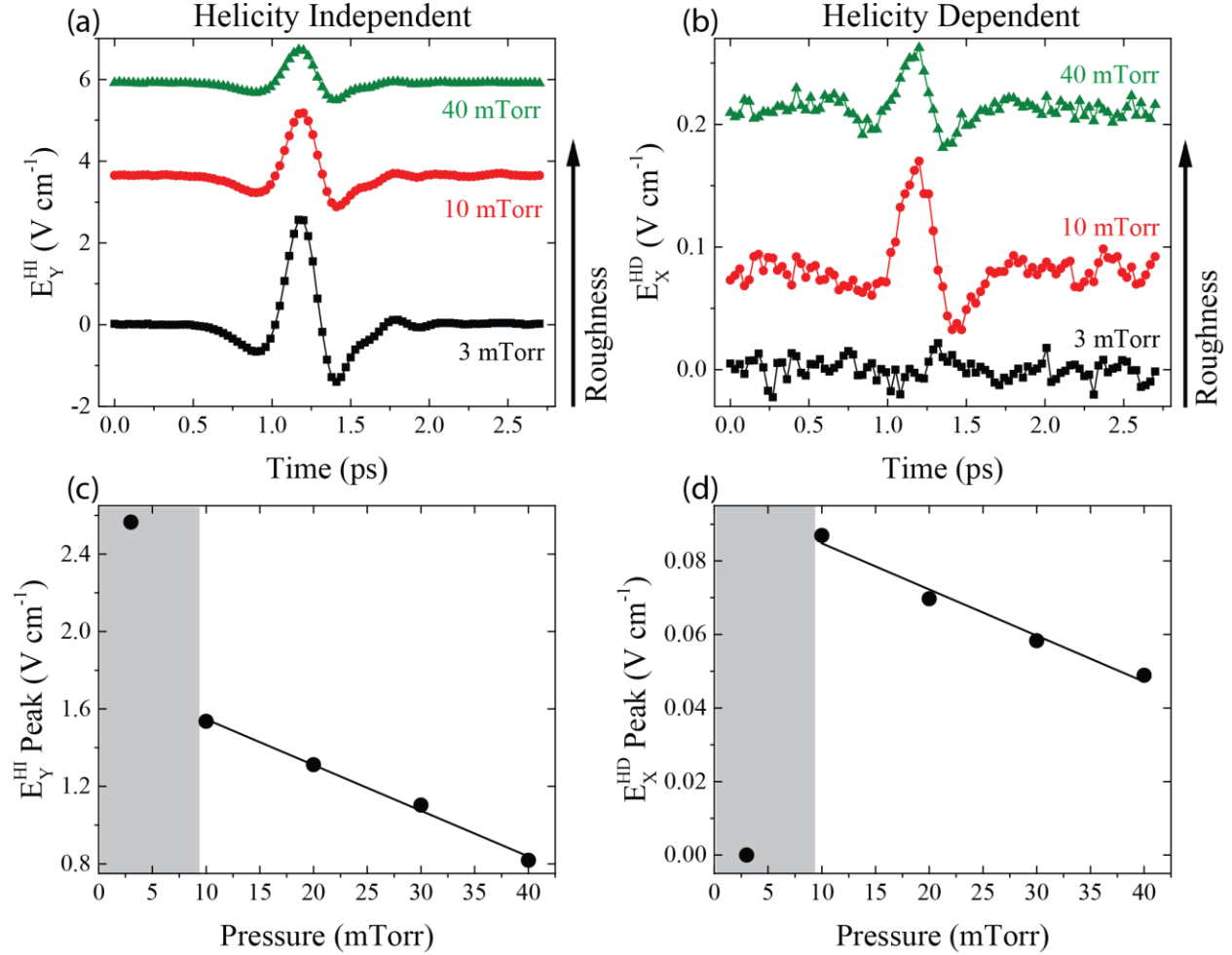


Figure 5 (a) The helicity-independent and (b) helicity-dependent THz emission for various interfacial roughness values. The time traces are shown with a vertical off-set. The observed electric field at 0 ps is 0 for the measurements. Peak intensities of (c) the helicity-independent THz and (d) helicity-dependent THz emission. The gray area emphasized deviations in the behavior. Beyond the gray area (10 mTorr) both the helicity-independent and dependent THz emission decreases linearly with increasing deposition pressures. The solid line is a guide to the eye.

To probe the role of the sample structure on the generation of HD and HI photocurrents, we measured the THz electric field from the Co/Pt samples described above. We initially studied smooth polycrystalline Co/Pt bilayers grown at 3 mTorr on glass substrates (Fig. 2(a)). The results of the experiment are shown in Fig. 5 for HI THz (panel a) and HD THz (panel b), respectively. Similar to previous works, the figure reveals a strong HI signal at 3 mTorr [24,38]. However, the bilayer grown at 3 mTorr does not show any HD THz signal (see Fig. 5(b)). An increase of the sputter pressure, that results in an increase of the structural disorder/interfacial roughness, changes the THz emission substantially. While an increase of the sputter pressure

results in a decrease of the HI THz signal, an increase of the pressure from 3 mTorr to 10 mTorr results in a dramatic increase of the HD THz signal. Further increase of the pressure above 10 mTorr results in a decrease of the HD signal, similar to the HI signal. The peak amplitudes of the HI and HD THz signals are plotted versus Ar deposition pressure in Figs. 5(c,d). The jump in HD THz signal upon pressure increase from 3 mTorr to 10 mTorr highlights the importance of roughness for the mechanism of HD THz emission.

## (b) Intermixed Interface

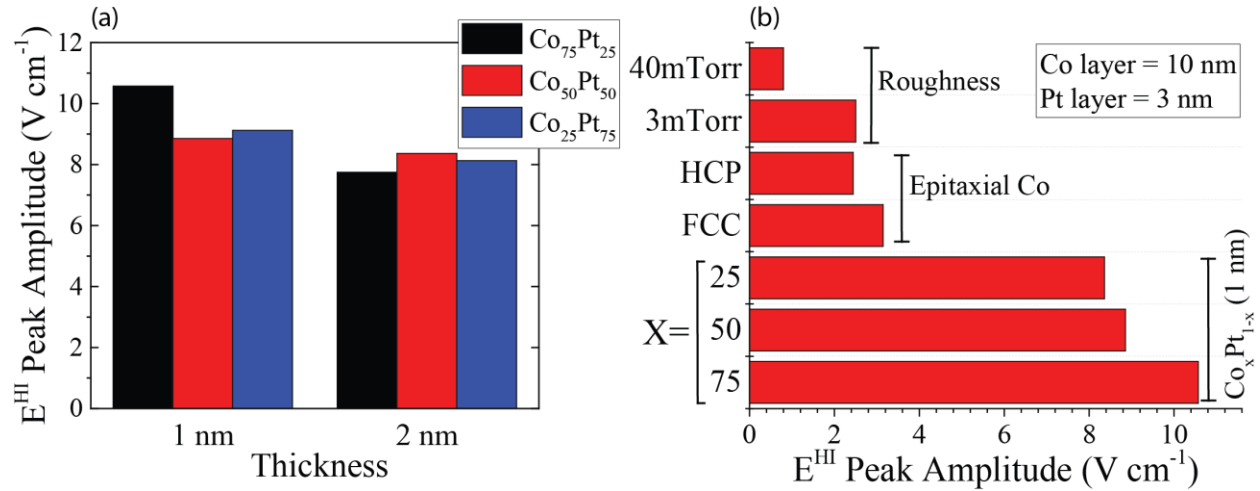


Figure 6 (a) The peak amplitude of the helicity-independent THz emission from samples with the  $\text{Co}_x\text{Pt}_{1-x}$  alloy spacers. The alloy compositions are  $\text{Co}_{75}\text{Pt}_{25}$  (black),  $\text{Co}_{50}\text{Pt}_{50}$  (red), and  $\text{Co}_{25}\text{Pt}_{75}$  (blue). (b) The peak amplitudes of the helicity-independent THz emission from samples with the  $\text{Co}_x\text{Pt}_{1-x}$  spacer in comparison with the helicity-independent THz signals from Co/Pt samples with the roughest (sputter pressure is 40 mTorr) and the smoothest (sputter pressure is 3 mTorr) Co/Pt interface as well as compared to the helicity-independent THz signal from Co/Pt samples with epitaxial HCP-Co and FCC-Co films.

To study the contribution of interfacial mixing we introduced a spacer layer of  $\text{Co}_x\text{Pt}_{1-x}$  alloy of various  $\text{Co}_x\text{Pt}_{1-x}$  compositions at the interface of the Co/Pt bilayers. The films were grown at 3 mTorr to have a smooth, but diffuse interface. We employed alloys of  $\text{Co}_{75}\text{Pt}_{25}$ ,  $\text{Co}_{50}\text{Pt}_{50}$ , and  $\text{Co}_{75}\text{Pt}_{25}$  with thicknesses of 1 and 2 nm. The experimental procedure was similar to the one performed on the rough Co/Pt interfacial bilayers. Surprisingly, no HD THz emission was observed for all the samples having a  $\text{Co}_x\text{Pt}_{1-x}$  spacer layer. The HI THz emission was nevertheless strong, but very much similar for all six samples (see Fig. 6(a)). Note that during the sample growth only the concentration of Co and Pt and the sputtering time were varied, all other parameters were kept constant. One can see from Fig. 6(a) two noticeable differences in the peak amplitudes of the HI THz emissions. Firstly, the THz peak amplitude shows a decrease with increasing layer thickness. Secondly, for the sample with 1 nm spacer one can notice a decrease of the THz peak amplitude with increasing Pt concentration. The dependence of the THz peak amplitude becomes monotonous when we increased the thickness of the spacer layer to 2 nm. We compared the HI THz signal from samples with a  $\text{Co}_x\text{Pt}_{1-x}$  spacer and without a  $\text{Co}_x\text{Pt}_{1-x}$  spacer (Co/Pt bilayers with the roughest and the smoothest interfaces as well as with the epitaxial HCP-Co and FCC-Co layers), these results are shown in Fig. 6(b). We find a dramatic

increase in the HI THz emission with insertion of an alloy interlayer when compared to the reference Co/Pt structure.

### (c) Epitaxial FCC-Co and HCP-Co(10 nm)

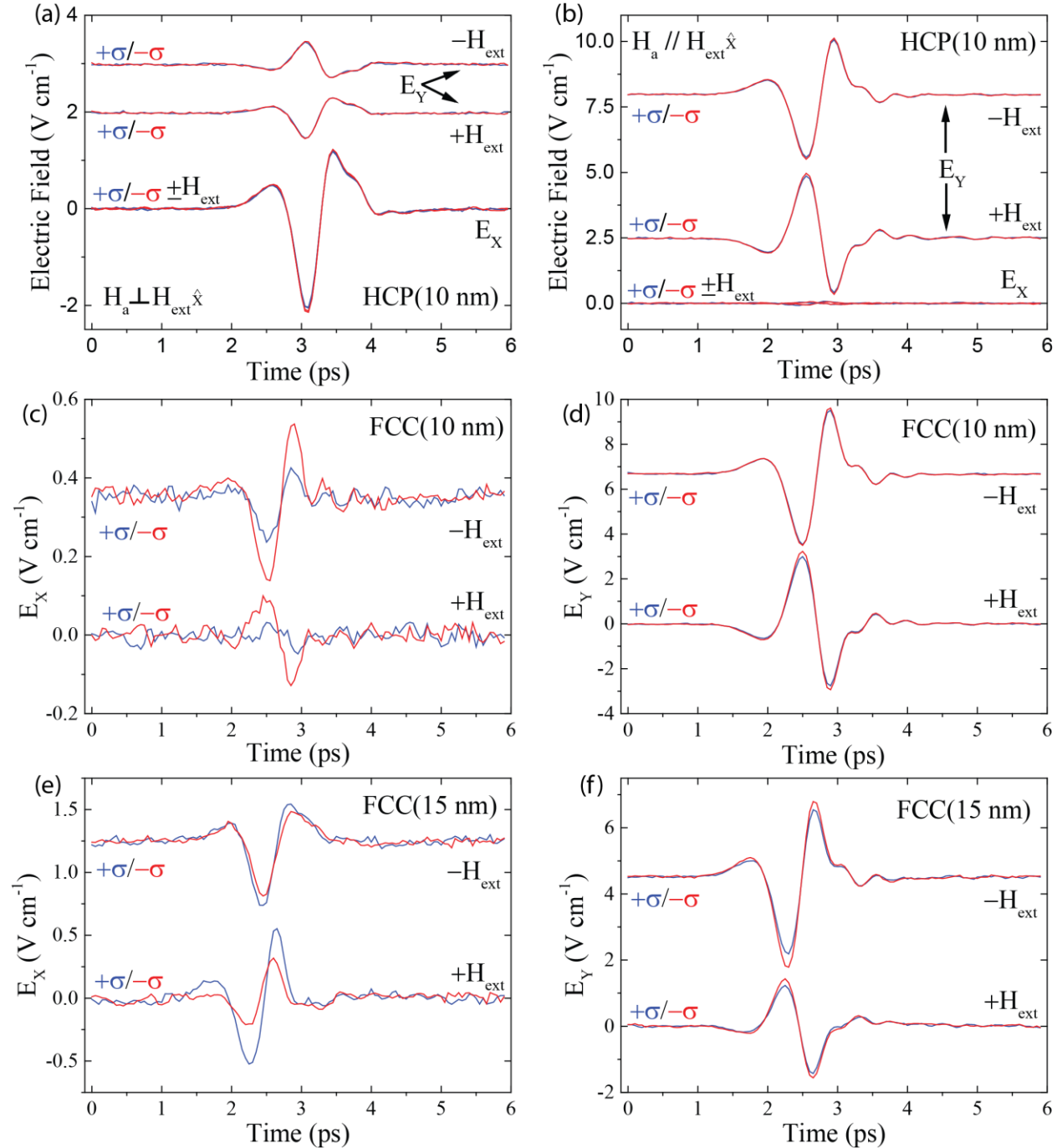


Figure 7 Time traces of the THz electric field polarized along the  $\hat{x}$  and  $\hat{y}$  axes. The emission was generated by exciting Co/Pt bilayers with monocrystalline (HCP and FCC) Co with circularly ( $+\sigma/-\sigma$ ) polarized laser pulses. The external magnetic field ( $\pm H_{ext}$ ) is applied along the  $\hat{x}$ -axis. The easy axis of the magnetic anisotropy ( $H_a$ ) of HCP-Co is aligned either (a) perpendicular or (b) parallel to the external magnetic field. The THz emission polarized along the  $\hat{x}$ - and  $\hat{y}$ -axis for (c,d) FCC-Co(10 nm) and (e,f) FCC-Co(15 nm), respectively.

Finally, we studied the role of the crystal structure of Co at the Co/Pt interface in the process of THz emission. No HD THz emission was observed from the samples with monocrystalline Co, while the HI THz emission manifestation of the crystal structure of the Co film was clearly seen. The crystalline orientation in our HCP-Co sample is (10-10). Due to the crystal structure, the material acquires in-plane magnetic anisotropy with the hard and in-plane easy axis along the [0001] and [1120] directions, respectively. We therefore studied the THz emission for two cases where the magnetic field was parallel and perpendicular with respect to the easy axis. The magnetic anisotropy of Co had a remarkable effect on the THz emission. Figs. 7(a,b) shows the time traces of the THz electric field for the case when the external magnetic field ( $H_{\text{ext}}$ ) is perpendicular and when it is parallel to the easy axis of the magnetic anisotropy ( $H_a$ ). The external magnetic field of 0.1 T was strong enough to saturate the magnetization along the easy axis (parallel to the magnetic anisotropy). However, it was too weak to fully saturate the magnetization along the hard axis (perpendicular to the magnetic anisotropy). This is reflected in the magnetic hysteresis loops shown in Fig. 3(g). The polarization of the detected THz signal ( $E_y$ ) along the  $\hat{y}$ -axis, perpendicular to the external magnetic field ( $H_{\text{ext}}$ ), showed a reversal of the THz field sign upon switching the polarity of the external magnetic field. However, the polarization of the detected THz signal ( $E_x$ ) along the  $\hat{x}$ -axis, parallel to external magnetic field, becomes insensitive to the polarity of the magnetic field.

In the case of the FCC-Co, it has a weak four-fold in-plane magnetic anisotropy with a strong out-of-plane shape anisotropy along the [001] direction (see Fig. 3(h)). The external magnetic field was also strong enough to saturate the in-plane magnetization. For this case we studied two FCC-Co layers with a thickness of 10 nm and 15 nm. Figs. 7(c,d) shows the time traces of the detected THz signal of FCC-Co(10 nm) with its polarization parallel ( $E_x$ ) and perpendicular ( $E_y$ ) to the external magnetic field, respectively. Similarly, Figs. 7(e,f) shows the time traces of the THz signals of FCC-Co(15 nm). The THz signal ( $E_y$ ) polarized perpendicular to the external magnetic field showed no clear difference between the FCC-Co(10 nm) and HCP-Co(10nm) samples. However, we observed an asymmetry with respect to the magnetic field polarity in the  $E_y$  THz signal of the FCC-Co(15 nm) sample (see Fig. 7(f)). For the detected THz signal ( $E_x$ ) polarized parallel to the external magnetic field we observed both dependence on the helicity of light as well as the magnetic field. However, this effect (see Figs. 7(c,e)) is different from the HD effect as shown in Fig. 4(b).

## **(5) Discussion**

### **(a) HI THz Emission**

By varying the deposition pressure during the Co growth process, we have demonstrated that one could control surface and interface roughness of Co/Pt bilayers. From the static magnetometry data, shown in Fig. 2, we observed a strong increase in the coercivity of the in-plane magnetization between the Co layer grown at 3 mTorr and 10 mTorr, while a strong decrease in the out-of-plane saturation of the magnetization was observed. The change in the

magnetic characteristics between 3 mTorr and 10 mTorr indicated how the roughness can have a strong influence on the magnetization of Co. This is reflected in the HI THz signal shown in Figs. 5(a,c).

Very recently, Bonetti *et al.* [39] demonstrated that a single cycle THz field induced electric current behaves distinctly different in metallic magnetic thin films that are similar magnetically, but different structure-wise. The interaction of an intense THz field pulse with a magnetic film drives instantaneous spin-polarized currents in the film [40]. It has been shown that such spin-polarized currents, within the duration of the THz pulse, only induce a field-like torque to trigger magnetic precession in structurally ordered Fe thin films. However, in the case of amorphous CoFeB thin films the magnetic precession was found to be preceded by an ultrafast demagnetization process. This additional demagnetization was attributed to the spin-lattice scattering processes at the defects that are readily available in the amorphous film. Similarly, our experiments on the Co roughness revealed a dramatic change in the peak amplitudes of the THz signals when the arrangement of Co atoms in the film was varied from a more ordered to a granular like arrangement. The HI THz signal, related to the ultrafast demagnetization of Co in the Co/Pt bilayer, showed a drastic decrease in its peak amplitude when increasing the disorder of Co grown at 3 mTorr to Co grown at 10 mTorr.

In the intermixing experiment with the  $\text{Co}_x\text{Pt}_{1-x}$  spacer layers, only small differences in the HI THz signal were observed (see Fig. 6(a)). The decrease in THz emission signal with thicker spacer layer can be explained due to the increased separation between the Co and Pt layers, this is consistent with the observations in Co/ZnO/Pt and Co/Cu/Pt multilayers [38]. However, the HI THz signal generated in Co/Pt bilayers with the  $\text{Co}_x\text{Pt}_{1-x}$  spacer is much stronger compared to the HI THz signal generated in Co/Pt with various roughness or crystal structure (see Fig. 6(b)). The HI THz peak signal generated from Co/Co<sub>75</sub>Pt<sub>25</sub>(1 nm)/Pt was more than three times larger than the HI THz peak signal generated from the smoothest interfacial Co/Pt as well as from the samples with FCC/HCP grown Co/Pt. This interface-dependent mechanism for the optimization of the THz emission has not been discussed before and thus reveals new opportunities for further increase of the intensity of the THz radiation from Co/Pt and similar multilayers [10-14].

For the HI THz signal from the epitaxially grown Co multilayers we observed clear differences between FCC-Co and HCP-Co. In the case of HCP-Co, when the easy axis of the magnetic anisotropy was parallel to the magnetic field, the HI THz signal sign, polarized perpendicularly to the magnetic field, is sensitive to the polarity of the magnetic field (see Fig. 7(b)). The THz signal polarized parallel to the magnetic field is fully suppressed. When the easy axis was perpendicular to the magnetic field, then the HI THz signal sign, polarized perpendicular to the magnetic field, is also sensitive to the polarity of the magnetic field (see Fig. 7(a)). However, the THz signal amplitude is reduced with respect to the previous case. We also observed a THz signal polarized parallel to the magnetic field with a peak amplitude comparable with respect to the THz signal in Fig. 7(b). Surprisingly, the sign of the THz signal was insensitive to the polarity of the magnetic field. This means that the THz polarization was tilted at an angle  $\pm\theta$  with respect to the  $\hat{x}$ -axis. This can be explained qualitatively from the perspective that the magnetic anisotropy which determines the spin orientation of the spin current is rotated with respect to the easy axis due to the external magnetic field. Therefore, the spin-Hall effect which in turn

determines the direction of the charge current will also change its direction. If the easy axis of the magnetic anisotropy lies parallel with respect to the magnetic field, the polarity of the magnetic anisotropy can be easily switched. This results in the sensitivity of the THz signal to the magnetic field. However, when the easy axis is perpendicular to the magnetic field, the magnetization of Co cannot be saturated along the magnetic field. Therefore, the THz emission sensitive to the polarity of the magnetic field will be reduced being scaled with respect between the external magnetic field and the magnetic saturation field. In any case, the THz polarization perpendicular to the magnetization will be insensitive to the polarity of the external magnetic field.

## **(b) HD THz Emission**

Our experiments revealed the crucial importance of interfacial roughness for the generation of HD THz emission. We observed that HD THz emission emerges abruptly at a critical interfacial roughness of 0.3 nm, obtained for growth at deposition pressure of 10 mTorr, see Fig. 5(b). Note that temporal profiles of the electric field for both HI and HD THz emission are similar for samples with different roughness. At the same time, according to Kuiper *et al.* [41] if any change of the growth procedure would result in an effective change of the spin-orbit interaction, one would expect a change of characteristic times of the laser-induced magnetization dynamics accompanied by a change of the temporal profile of the emitted THz electric fields. Hence we propose that the observed increase of the efficiency of the THz emission upon an increase of the interface roughness is due to geometrical increase of the volume of the area that has the properties of the interface.

Our next approach was to determine whether  $\text{Co}_x\text{Pt}_{1-x}$  intermixing or crystalline structure at the rough interface play a role in the HD THz generation. Our finding on the  $\text{Co}_x\text{Pt}_{1-x}$  alloy spacer samples, simulating the intermixing effect, showed that while the intermixing enhanced the HI THz emission, it plays no role in the generation of HD THz emission.

From the epitaxially grown Co layer samples, we saw no clearly defined HD THz signal in either FCC or HCP structures. The THz emission in the HCP structure mainly originates from the spin-Hall effect. However, in FCC-Co we observed small dependences of the helicity of light on the THz emission (see Figs. 7(c,e)), but full sensitivity comparable to the HD signal shown in Fig. 4(b) from the Co/Pt roughness experiment was not achieved. We do not rule out the possibility that the small differences in the HD THz signals are due to artifacts such as leakage of the electric field from the wire-grid polarizers. This also further demonstrates negligible influence of spin-orbit coupling assisted demagnetization in epitaxially grown Co films.

## **(6) Conclusion**

In conclusion, we have studied the THz emission from Co/Pt bilayers grown at various deposition pressures. A relatively high interfacial roughness in Co/Pt is crucial for the generation of helicity dependent THz emission. The study of the THz emission from Co/Pt samples with  $\text{Co}_x\text{Pt}_{1-x}$  spacer layers at various  $\text{Co}_x\text{Pt}_{1-x}$  compositions and thicknesses showed that the intermixing of Co/Pt at the interface does not play a role in the generation of helicity-dependent THz emission. However, it plays a significant role in amplifying the helicity-

independent THz emission. The observed THz signal from the Co/ Co<sub>x</sub>Pt<sub>1-x</sub>/Pt trilayers were significantly larger compared to the THz signal from Co/Pt bilayers. Finally, we observed a dramatic suppression of the helicity-dependent THz emission in Co/Pt with crystalline FCC or HCP-Co compared to the case with an amorphous Co layer. Therefore, these observations show that the helicity-dependent THz emission is the strongest for the cases of rough Co/Pt interfaces with amorphous Co and no intermixing of Co and Pt. While the strongest helicity-independent THz emission must be expected for smooth Co/Pt interfaces with intermixing of Co and Pt. In none of the THz emission mechanisms crystal structure of Co seems to play a significant role.

## (7) Acknowledgements

This work was funded by DOE grant #DE-SC001823, the Nederlandse Organisatie voor Wetenschappelijk Onderzoek (NWO), the European Union Horizon 2020 and innovation program under the FET-Open grand agreement no.713481 (SPICE), the European Research Council ERC grant agreement no.339813 (EXCHANGE), the ministry of Education and Science of the Russian Federation project no.14.Z50.31.0034, and the Russian Science Foundation 16-12-10520. We want to thank Ray Descoteaux from CMRR, Sergey Semin, Tonnie Toonen, and Chris Berkhout from Radboud university for all the technical support.

## (8) References

- [1] A. Kirilyuk *et al.* *ultrafast optical manipulation of magnetic order*. Reviews of modern Physics **82**, 2731-2784 (2010).
- [2] J. Walowski *et al.* *Perspective: Ultrafast magnetism and THz spintronics*. Journal of Applied Physics **120**, 140901 (2016).
- [3] P. Nemec *et al.* *Antiferromagnetic opto-spintronics*. Nature Physics **14**, 229-241 (2018).
- [4] E. Beaurepaire *et al.* *Ultrafast spin dynamics in ferromagnetic Nickel*. Physical Review Letters **76**, 4250 (1996).
- [5] B. Koopmans *et al.* *Ultrafast magneto-optics in Nickel: Magnetism or optics?* Physical Review Letters **85**, 844 (2000).
- [6] K. Carva *et al.* *Is the controversy over femtosecond magneto-optics really solved?* Nature Physics **7**, 665 (2011).
- [7] E. Beaurepaire *et al.* *Coherent terahertz emission from ferromagnetic films excited by femtosecond laser pulses*. Applied Physics Letters **84**, 3465 (2004).
- [8] D. J. Hilton *et al.* *Terahertz emission via ultrashort-pulse excitation of magnetic metal films*. Optics Letters **29**, 1805 (2004).
- [9] T. J. Huisman *et al.* *Simultaneous measurements of terahertz emission and magneto-optical Kerr effect for resolving ultrafast laser-induced demagnetization dynamics*. Physical Review B **92**, 104419 (2015).

- [10] T. Kampfrath *et al.* *Terahertz spin current pulses controlled by magnetic heterostructures.* Nature Nanotechnology **8**, 256-260 (2013).
- [11] Yang Wu *et al.* *High-performance THz emitters based on ferromagnetic/nonmagnetic heterostructures.* Advanced Materials **29**, 1603036 (2017).
- [12] D. Yang *et al.* *Powerful and tunable THz emitters based on the Fe/Pt Magnetic Heterostructure.* Advanced Optical Materials **4**, 1944-1949 (2016).
- [13] T. Seifert *et al.* *Efficient metallic spintronic emitters of ultrabroadband terahertz radiation.* Nature Photonics **10**, 483-488 (2016).
- [14] T. Seifert *et al.* *Ultrabroadband single-cycle terahertz pulses with peak fields of  $300 \text{ kV cm}^{-1}$  from a metallic spintronic emitter.* Applied Physics Letters **110**, 252402 (2017).
- [15] G. Ju *et al.* *Ultrafast nonequilibrium spin dynamics in a ferromagnetic thin film.* Physical Review B **57**, R700 (1998).
- [16] P.J. Bennett *et al.* *Femtosecond cubic optical nonlinearity of thin nickel films.* Optics Letters **24**, 1373 (1999).
- [17] R. Wilks *et al.* *Investigation of ultrafast demagnetization and cubic optical nonlinearity of Ni in the polar geometry.* Journal of Applied Physics **95**, 7441 (2004).
- [18] A.V. Kimel *et al.* *Ultrafast non-thermal control of magnetization by instantaneous photomagnetic pulses.* Nature **435**, 655-657 (2005).
- [19] N.P. Duong *et al.* *Ultrafast manipulation of antiferromagnetism of NiO.* Physical Review Letters **93**, 117402 (2004).
- [20] F. Hansteen *et al.* *Femtosecond photomagnetic switching of spins in ferrimagnetic garnet films.* Physical Review Letters **95**, 047402 (2005).
- [21] C.D. Stanciu *et al.* *All-optical magnetic recording with circularly polarized light.* Physical Review Letters **99**, 047601 (2007).
- [22] A.V. Kimel *et al.* *Picosecond Dynamics of the Photoinduced Spin Polarization in Epitaxial (Ga,Mn)As Films.* Physical Review Letters **92**, 237203 (2004).
- [23] N. Kanda *et al.* *The vectorial control of magnetization of light.* Nature Communications **2**, 236 (2011).
- [24] T.J. Huisman *et al.* *Femtosecond control of electric currents in metallic ferromagnetic heterostructures.* Nature Nanotechnology **11**, 455-458 (2016).
- [25] J. A. Thornton *et al.* *The microstructure of sputter-deposited coatings.* Journal of Vacuum Science and Technology A **4**, 3059 (1986).
- [26] E. E. Fullerton *et al.* *Interfacial roughness of sputtered multilayers: Nb/Si.* Physical Review B **48**, 17432 (1993).



- [27] P. He *et al.* *Sputtering pressure effect on microstructure of surface and interface, and on coercivity of Co/Pt multilayers.* Journal of Applied Physics **70**, 6044 (1991).
- [28] M. Grimsditch *et al.* *Exchange and anisotropy effects on spin waves in epitaxial Co films.* Physical Review B **56**, 2617-2622 (1997)
- [29] M. Ohtake *et al.* *preparation and characterization of Co single-crystal thin films with hcp, fcc, and bcc structures.* Journal of Applied Physics **109**, 07C105 (2011).
- [30] T.J. Huisman *et al.* *Spin-photo-currents generated by femtosecond laser pulses in a ferromagnetic GdFeCo/Pt bilayer.* Applied Physics Letters **110**, 072402 (2017).
- [31] G.M. Choi *et al.* *Spin current generated by thermally driven ultrafast demagnetization.* Nature Communications **5**, 4334 (2014).
- [32] M. Battiato *et al.* *Theory of laser-induced ultrafast superdiffusive spin transport in layered heterostructures.* Physical Review B **86**, 024404 (2012).
- [33] K. Ando *et al.* *Inverse spin-Hall effect induced by spin pumping in metallic system.* Journal of Applied Physics **109**, 103913 (2011).
- [34] K. Garello *et al.* *Symmetry and magnitude of spin-orbit torques in ferromagnetic heterostructures.* Nature Nanotechnology **8**, 587-593 (2013).
- [35] G.M. Choi *et al.* *Optical-helicity-driven magnetization dynamics in metallic ferromagnets.* Nature Communications **8**, 15085 (2017).
- [36] A. Manchon *et al.* *Theory of spin torque due to spin-orbit coupling.* Physical Review B **79**, 094422 (2009).
- [37] F. Freimuth *et al.* *Laser-induced torques in metallic ferromagnets.* Physical Review B **94**, 144432 (2016).
- [38] G. Li *et al.* *Laser induced THz emission from femtosecond photocurrents in Co/ZnO/Pt and Co/Cu/Pt multilayers.* Journal of Physics D **51**, 134001 (2018).
- [39] S. Bonetti *et al.* *THz-driven ultrafast spin-lattice scattering in amorphous metallic ferromagnets.* Physical Review Letters **117**, 087205 (2016).
- [40] Z. Jin *et al.* *Accessing the fundamentals of magnetotransport in metals with terahertz probes.* Nature Physics **11**, 761 (2015).
- [41] K.C. Kuipers *et al.* *Spin-orbit enhanced demagnetization rate in Co/Pt multilayers.* Applied Physical Letters **105**, 202402 (2014).